Paper No.
327

CORROSION 93
The NACE Annual Conference and Corrosion Show

COMPUTATION OF REINFORCING STEEL CORROSION DISTRIBUTION IN CONCRETE MARINE BRIDGE SUBSTRUCTURES

S.C. Kranc and A.A. Sagüés
Department of Civil Engineering and Mechanics
University of South Florida
Tampa, Florida 33620

ABSTRACT

The corrosion conditions prevalent in the partially submerged reinforced concrete substructure of marine bridges have been incorporated in a computer model. The system modeled is an axisymmetric cylindrical column with a rebar cage placed along its entire length. Inputs to the model include the column and cage dimensions, the size of the portion of the rebar cage which is in an active state, the concrete resistivity and oxygen diffusivity distributions along the column, the polarization characteristics of the steel, and the external oxygen concentration. A finite difference model was used to compute the distribution of electrical potential and oxygen concentration throughout the system. From these results are obtained the distribution of oxygen consumption and corrosion current densities over the rebar cage. Cases addressing various dimensions, and various distributions of oxygen diffusivity and concrete resistivity are analyzed. For the parameters tested, the results show a tendency for greatest corrosion near the top of the active zone, and that relative changes in oxygen diffusivity have a greater impact on corrosion activity than comparable relative changes in concrete resistivity. Implications for marine substructures are examined.
Keywords: Corrosion, concrete, reinforcing steel, computer, computation, model, substructures, marine, oxygen, chloride, bridges, finite difference.

INTRODUCTION

Steel-reinforced concrete is frequently used to build substructure members in marine bridges. The lower substructure may include piles made of concrete containing prestressed steel strands, or

drilled shafts of concrete reinforced with steel bars. A reinforced concrete footer is often placed on top of the lower elements, and reinforced concrete columns may be built on top of the footer. Horizontal reinforced concrete struts are sometimes used to join adjacent columns. The lower portion of the substructure is often permanently submerged in seawater, and the region immediately above is subject to tidal variations in the local sea level. The substructure above the high tide line experiences wave splash, seawater mist and occasional wash due to the wakes of watercraft traffic. Depending on the local conditions, the latter action may result in seawater contact reaching portions of the bridge superstructure.

The water solution present in concrete pores is initially highly alkaline (pH near 13 [1]) and the steel embedded in the concrete becomes passivated as a result. However, passivity breakdown can take place if chloride ions from the external seawater penetrate through the concrete cover. Various investigations indicate that passivity loss occurs when the concentration of chloride ions in the pore solution is of the same order as the hydroxide ion concentration [1-3]. With typical concrete formulations and cover thicknesses, it is not uncommon to observe the onset of active corrosion in marine bridge substructures after only a few years of service. Steel depassivation is by no means limited to the portion of the structure that is always submerged. Indeed, chloride buildup is faster and more pronounced in the region directly above the high tide line. This is due to evaporation of the seawater between wetting events, leading to chloride enrichment of the solution remaining absorbed at the concrete surface and a consequent increase in the quantity of chloride ion diffused inward.

After depassivation of the steel, the distribution of corrosion in Florida coastal marine substructures tends to develop a maximum in a region typically 0.5m to 2m above the high tide mark [4]. Several factors are thought to act jointly in creating this situation. Early accumulation of chloride above high tide should allow for longer evolution times in the process of corrosion product accumulation and subsequent cracking that characterizes reinforcement corrosion damage [2,3]. Perhaps more important are the roles of the distribution of the cathodic reaction and of the electrolyte resistance along the substructure elements.

The main cathodic reaction responsible for reinforcement corrosion is considered to be oxygen reduction [5]. Oxygen is transported through the concrete cover to the surface of the reinforcing steel. Oxygen reduction can proceed readily even if the surface of the steel is passive, so the reaction is not limited to those areas of the steel in contact with chloride ions. While there is only limited experimental evidence available, it is generally thought that oxygen transport is much faster in dry than in water-saturated concrete. Measurements by Tuutti [6] indicate a three orders of magnitude difference in the effective diffusion coefficient of oxygen in concrete exposed to 100% relative humidity (R.H.) air versus concrete exposed to dry air. If the rate of the cathodic reaction were subject to simple transport limitation, the cathodic current density would then be expected to be greatest in the regions above water.

The anodic reaction would first take place in the area of chloride concentration above the waterline. Later, anodic dissolution would be possible also in the entire submerged portion of the column, where the chloride content will have reached the critical level for depassivation. A corrosion macrocell pattern may then develop, with the cathodic reaction predominant above water, and anodic processes taking place in all the regions where steel passivity was lost. However, as indicated above corrosion is usually less important in the permanently submerged portion of the substructure. The finite resistivity of concrete may provide an explanation for this behavior.

Hardened concrete is a highly inhomogeneous medium, composed of cement paste in which fine aggregate (typically sand) and coarse aggregate (stone, often with sizes in the 2 cm range) are mixed. Oven-dry concrete behaves much as an electrical insulator, but in the presence of common ambient air enough water is present in the cement paste and aggregate pores to result in significant conduction. Thus, resistivities on the order of 10 KΩ-cm to 1 MΩ-cm are often observed in ambient air for concrete specimens large enough to average out local inhomogeneities. Water-saturated concrete has resistivities typically in the 1-10 KΩ-cm range [7,8]. The concrete resistivity results in finite resistance paths between the constituents of the corrosion macrocell. Since the cathodic reaction is expected to be taking place primarily above water, the effective circuit resistance is thought to be high enough so that the anodic reaction rate cannot be large much below the waterline. In the portion of the column above water similar IR drop effects may result on the cathodic reaction being of importance for only a limited distance above the active region of the reinforcement.

The factors determining corrosion current distribution in these systems can be understood qualitatively. However, the complexity of the geometric, physical and electrochemical factors involved prevents applying limited qualitative arguments to specific engineering questions. For example, it might be of interest to know how much will the total rate of corrosion be changed if the concrete resistivity is doubled. Likewise, it may be argued that the seawater surrounding the submerged region may, in some cases, provide enough parallel conductance to extend the macrocell action significantly below the waterline.

The purpose of this paper is to present a computational model of substructure conditions that can address quantitatively the main operating conditions of the system, and subject to numerical test the expectations of previous qualitative assessments. The computational approach used contains features of earlier models by the authors and others [9-12].

APPROACH

The calculations are based on a vertical, cylindrical reinforced concrete column, with its lower part immersed in seawater (Figure 1). The entire system is axisymmetric. The column contains a single cylindrical reinforcing steel cage, with a radius equal to that of the column minus the thickness of the concrete cover. For the purpose of these calculations, the reinforcing steel cage will be treated as a screen with mesh spacing much smaller than the dimensions of the rest of the system. In effect, the rebar cage will be considered as a two-sided pervious sheet. This represents a simplification from the discrete bar lattice geometry (which has a typical characteristic spacing on the order of 1/4 of the column diameter). Nevertheless this simplification permits the evaluation of general corrosion distribution trends and the corrosion macrocell pattern of the column.

The concrete is treated as a radially homogeneous conducting electrolyte with variable conductivity along the column axis. The concrete is also treated as a medium where oxygen can be transported by diffusion. Both resistivity and oxygen diffusivity are considered constant in the radial direction but variable along the column axis. It is assumed that oxygen concentration in the column medium is constant along the entire external cylindrical surface, for both the upper and submerged portions of the column. For simplicity, oxygen flow across the upper and lower end surfaces of the column is considered to be zero.

The rebar cage surface is considered to be active in a region that includes the entire submerged portion and a length reaching from the waterline to a preset height. The latter region is representative of the rebar zone above water where chloride contamination has reached the threshold for active corrosion. The rest of the cage is treated as a passive surface, which is treated as the site of cathodic reaction (oxygen reduction: $O_2+2H_2O+4e \rightarrow 4OH^-$) only. Active surfaces support both the cathodic reaction and the anodic reaction (iron dissolution: $Fe \rightarrow Fe^{++}+2e$).

Reverse reactions (oxygen evolution and iron reduction) are considered to be negligible for the operating potential regime present in the column. The polarization behavior of the anodic and cathodic reactions will be assumed to be determined by simplified electrode kinetics:

$$i_{Fe} = i_{o\,Fe} \exp[2.3(E_s-E_{o\,Fe})/b_a] \quad (1)$$

$$i_{OR} = i_{o\,OR} (C_s/C_O) \exp[2.3(E_{o\,OR}-E_s)/b_c] \quad (2)$$

(symbols are explained in the Nomenclature section.)

Eq.(1) assumes that the anodic reaction is subject only to simple activation polarization (unrestricted metal supply). Eq.(2) takes into consideration both activation and concentration polarization effects for the oxygen reduction reaction.

The two-sided sheet approximation corresponds to a steel placement density of 2 m^2 of steel surface for every 1 m^2 of nominal mat area. Actual placement densities in structures are typically closer to 1 m^2:1 m^2. Examination of the system conditions shows that a 1:1 placement density can be simulated by using exchange current densities in Eqs. (1) and (2) that are one-half the value of those encountered on an actual steel surface. The same considerations show that for a 1:1 placement density the actual average current densities of the reactions on the steel surface can be simulated by adding the computed current densities on both sides of the pervious sheet. To better represent an actual system, the 1:1 steeel placement density will be simulated in the present calculations by means of the scaling procedure just described. Other placement density values can be simulated if desired by using the appropriate scaling factors.

For the purpose of evaluating the polarization conditions at every point of the rebar cage, the volume of the column is divided into axisymmetric regions defined by divisions along the radial and longitudinal directions (see Figure 1). The radius is divided into 35 zones (36 radial nodes), and the column length into 240 zones (241 longitudinal nodes). The rebar cage is located at node 28, counting from the center (node 0).

The steady state current distribution within the concrete is calculated by solving the continuity equation:

$$\nabla \mathbf{i} = 0 \quad (3)$$

since by Ohm's law:

$$\mathbf{i} = -\sigma \nabla E \quad (4)$$

the continuity equation becomes:

$$\nabla (\sigma \nabla E) = 0 \qquad (5)$$

Note that Eq.(5) would reduce to the Laplace equation, $\nabla^2 E = 0$ (commonly used in previous calculations of corrosion current distributions in concrete [9-12]) if σ were constant.

The boundary conditions for Eq.(5) at the rebar cage are provided by the polarization conditions, Eqs. (1) and (2). Each element of the rebar cage is considered as a two-sided surface. The electrolyte potential is a continuous function along a direction crossing the cage, so E is the same (E_s) on either side immediately next to the cage. On either side, the component of current density in the electrolyte normal to the surface will be given by

$$\mathbf{i}|_n = i_{Fe} - i_{OR} \qquad (6)$$

and by application of Eq.(4)

$$\Sigma_{\text{both sides}}(-\sigma \nabla|_n E) = \Sigma_{\text{both sides}}(i_{Fe} - i_{OR}) \qquad (7)$$

At the two column ends current flow is assumed to be zero so that

$$\nabla|_z E = 0 \quad \text{(column end faces)} \qquad (8)$$

Likewise, current flow is taken as zero perpendicular to the external column surface above the waterline (air insulation) and perpendicular to the column axis along the axis itself (by symmetry):

$$\nabla|_r E = 0$$

$$\text{(column exterior above water and } r=0) \qquad (9)$$

The portion of the column below water is in contact with an electrolyte that is typically two orders of magnitude more conductive than the adjacent concrete. This permits using a convenient approximation to an otherwise difficult boundary condition, by treating the surface in contact with seawater as a constant potential region:

$$E = \text{constant}$$

$$\text{(submerged column outer surface)} \qquad (10)$$

The oxygen distribution problem was addressed by taking into consideration that steady-state conditions prevailed. Therefore, at every point of the concrete, the oxygen concentration satisfied a condition similar to that of Eq. (5):

$$\nabla(D \nabla C) = 0 \qquad (11)$$

The oxygen supply, in turn, needs to equal the amount consumed by the cathodic reaction at the metal surface. Assuming that 4 electrons are consumed for each oxygen molecule:

$$\Sigma_{\text{both sides}}(i_{OR}) = \Sigma_{\text{both sides}}(4\ F\ \nabla|_n\ C) \quad (12)$$

The remaining boundary conditions were provided by the absence of oxygen transport at the column ends, and constant oxygen concentration at the sides.

$$\nabla|_n\ C\ |_{\text{ends}} = 0 \quad (13)$$

$$C|_{\text{sides}} = C_0 \quad (14)$$

Concrete is heterogeneous, and oxygen transport is expected to proceed through pores that are partially filled with water to an extent depending on the moisture content. The assumption of Fickian diffusion is at best an approximation, and the diffusion coefficient should be viewed as an effective magnitude. Reported measurements of effective diffusion coefficients of oxygen in concrete are derived from concentration gradients variously based on the oxygen content of air or of water in contact with the external concrete surfaces [5,6]. For the purposes of these calculations, it has been chosen to express C in terms the concentration of oxygen present in the pore solution, which is in turn assumed to be in equilibrium with any surrounding gas. The seawater is assumed to be in equilibrium with atmospheric oxygen within the depth range considered here [13]. For simplicity, both seawater and the pore solution were assumed to have oxygen solubilities (and associated pressure dependencies) equal to those of pure water.

The conditions expressed in Equations (1-14) were formulated as difference equations based on nodes placed on a longitudinal section of the column, representing the concrete in the column. The difference equations were formulated to account for cylindrical symmetry along the main axis, thus obtaining full spatial simulation. The equations were solved by means of a Gauss-Seidel method, stopping the iteration process when a predetermined maximum error criterion was met. For each internal node of the system, and at each iteration step, the new value of C was obtained from the surrounding values of the previous iteration, by Equation (11). The same procedure was used for E, using Equation (5) in the same step. At the appropriate boundaries, Equations (15,16) were applied consecutively at each node during the same step to obtain the new node values. Similar procedures were used for Equations (6-10).

RESULTS AND DISCUSSION

Cases Examined

Table I shows the cases examined. The baseline case consisted of a column with a total length of 1200 centimeters, half of which was above the water line. The active zone extended to 202.5 centimeters above the water line. The diffusion coefficient of oxygen varied along the column from a value $D_L = 10^{-5}$ cm^2/sec to a value $D_H = 10^{-3}$ cm^2/sec. Keeping in mind the gas-liquid equilibrium assumptions made above, these values correspond to the typical range of oxygen diffusivity reported in the literature [5,6]. Figure 1 shows the assumed pattern of variation of D along the column. Above water, the log of D was taken to vary linearly with height, to represent the expected rapid variation of D with moisture content [6]. The concrete resistivity was taken to vary from 2kΩ-cm to 10kΩ-cm. These resistivity values are in the range commonly observed in

actual substructure applications in humid environments. The variation was assumed to be linear with height above water, as a rough approximation to actual observed patterns [14]. The column diameter was 105cm, whereas the concrete cover over the rebar was 10.5cm. These values are representative of typical construction dimensions. The iron dissolution and oxygen reduction polarization parameters used in the calculations are also shown in Table I. These polarization parameters are equivalent to those used by the authors in previous computations [9-11], except that the exchange current densities are approximately halved to account for the two-sided sheet model as explained previously. In addition to the baseline, other cases investigated included variations in the height of the active zone above the water line, the height of the column above the water line, the diffusion coefficient limits and the concrete resistivity limits.

It is emphasized that the parameter ranges chosen for the calculations are intended only to obtain insight on the general patterns of corrosion behavior in the systems investigated. Specific dimensions and trends of parameter variation along the column could be very different from those assumed here, and detailed analysis of particular cases would require customized calculation with appropriate initial data.

The computations returned the value of the electrical potential and the oxygen concentration at every point in the concrete. From these values and by application of Equation (7), the distributions of the current along entering or leaving the rebar cage surface, and the amounts of oxygen consumed at various points of the system could be obtained. In addition, by application of Equation (1), the value of the corrosion current density could be obtained at any point where the surface of the rebar was active. Cathodic current densities will be treated as positive; anodic current densities will be treated as negative. The net current density flowing at any point from the rebar surface into the electrolyte will be denoted as the macrocell current density (which will be taken as positive). As indicated earlier, to account for the pervious sheet used to represent the rebar cage the results have been interpreted by taking at any point the sum of the process rates (current densities) of both sides of the mesh. The designation "sum of both sides" will be used as a reminder of this interpretation.

Potential and Oxygen Concentration Distributions

Figure 2 shows iso-electric potential and iso-oxygen concentration diagrams on longitudinal column cross-sections for the conditions of the baseline case A (note that in the convention used in the calculation the potentials are given with respect to the metal, so that less noble conditions correspond to higher potentials). The isopotential diagram shows that the potential increase as one moves from the air portion of the column to the submerged region. The increase reflects both the presence of the active region and the lower availability of oxygen in the wet portions of the column.

The isopotential lines indicate that there is a general flow of conventional current across the concrete from the lower to the upper parts of the column. This is because iron dissolution takes place only in the active, lower region while oxygen reduction is more predominant in the upper portion of the active zone and is the only reaction in the passive area. The resulting net ionic flow corresponds to the calculated conventional current direction.

The isoconcentration lines show predominant oxygen flow from the top to bottom in the upper part to the column, and from the exterior into the rebar cage in the lower regions. The

oxygen concentration is very low inside the cage over the entire active steel portion; in that region there is no significant oxygen transport through the interior of the column. In examining the diagram it should be remembered that the oxygen diffusivity is not constant along the column. Thus, although the isoconcentration lines show roughly the same spacing at the bottom of the passive region than in the region below water, the oxygen flow normal to the lines in the latter region is orders of magnitude smaller than in the former.

Current Distribution

The potential and concentration distributions discussed above, together with the conductivity and diffusivity distributions, define the extent of electrochemical reactions at the steel surface. The following discussion refers to current densities treated as the sum of both sides of the pervious sheet.

Figure 3 (top) shows the macrocell current density at points along the rebar cage as a function of position for the baseline case (A) and for a higher resistivity condition (B). The magnitude of the macrocell current density reaches a maximum at the highest active point of the column. At that location, the macrocell current also changes sign when going from the active portion to the passive portion of the column.

Figure 3 (center) shows the anodic current density (equal in magnitude but, by convention, opposite in sign to the corrosion current density) along the column. The corrosion current density reaches a maximum also at the highest active point in the column; the current density is zero (by assumption) at the passive region. The corrosion current density values obtained are typical of those encountered in reinforced concrete systems exposed to aggressive environments. The maximum corrosion current densities in Figure 3 would be enough to result in the observation of external cracks after several years of service [15] in that area of the column, in agreement with field observations. Nevertheless, the simplifications used in these calculations need to be kept in mind when interpreting these results.

Figure 3 (bottom) shows the cathodic current density (equal in magnitude and sign to the value of the oxygen consumption rate) at the rebar cage surface as a function of position along the column. The oxygen consumption is nearly constant for the entire submerged portion of the rebar cage, reflecting the assumption of constant oxygen diffusion coefficient in that region (where, as shown before, the oxygen supply is also under diffusion-limited conditions). The value computed by the model for the underwater oxygen consumption rate (0.12 $\mu A/cm^2$) is consistent with that obtained with an approximate calculation that would assume one-dimensional diffusion across the concrete cover: $i = 4\ F\ D\ C_O/c = 0.11\ \mu A/cm^2$. Oxygen consumption increases as elevations above the water line are reached, reflecting the increase in the diffusion coefficient as a function of height above the water line. However, the oxygen consumption begins to decay after a maximum at or near the highest point of the active zone. This behavior is a consequence of the electrical potential distribution on the rebar cage surface along the column. As indicated in Figure 2, the potential at the zone above the highest active spot tends to decrease in magnitude with further height, therefore reducing the demand for oxygen to the cathodic reaction.

Figure 3 also illustrates the effect of changing the value of the concrete electrical resistivity. As the electrical resistivity is increased by one order of magnitude (that is, going from case A to

case B), the distribution of the corrosion macrocell is confined to a smaller distance range. This is as expected, since the potential attenuation from the highest electrochemical activity point will be greater at greater electric resistivities. The same effect applies to the corrosion current density distribution. In addition, the maximum magnitudes of the corrosion current and macrocell current densities are smaller when the concrete resistivity is higher.

The effect of varying concrete resistivity on the oxygen consumption is more complex (Figure 3, bottom). Below the water line, the amount of oxygen demand does not change significantly upon increasing the resistivity, since that portion of the rebar cage behaves much as a uniform mixed-potential electrode. In that regime, oxygen transport is the limiting factor on the rate of corrosion, and resistivity has no significant effect. Above the water line, the increase in concrete resistivity results in a narrower transition region in the rate of oxygen consumption. The total rate of oxygen consumption is, as expected, lower for the high resistivity case. However, the peak value of the oxygen consumption rate tends to be actually slightly greater when the concrete resistivity is higher. This behavior is not surprising, since the peak rate results from a complex balance between the overall rate of the reactions and the size of the spacial region affected.

Corrosion Behavior Trends

Table II summarizes information that can be extracted from the results of all the cases computed. All magnitudes and rates correspond to the sum over both sides of the pervious sheet. The total macrocell current is equal to the absolute value of the integral of the macrocell current density over either the entire net anodic or the entire net cathodic portion of the column. The total corrosion current is equal to the absolute value of the integral of the corrosion current density over the entire active portion of the rebar cage surface. The maximum corrosion current density corresponds to the absolute value of the anodic current density at the highest point of the active zone. The oxygen consumption below water is the integral of the oxygen consumption rate over the portion of the rebar surface which lays below the water line. Finally, the iron solution rate below water results from integrating the corrosion current density over the portion of the rebar cage surface below the water line.

Figure 4 shows that increasing the concrete resistivity range (cases A,B,L,M) over more than an order of magnitude decreases the corrosion severity, but not to the same relative extent. The trend curves in the log-log representation can be approximated in the range investigated by straight lines, which in turn represent an approximate power relationship between the magnitudes examined:

$$I,i \propto \rho_L^{\,n} \qquad (15)$$

The slope of each line corresponds to the power exponent, n of each respective relationship. Thus, the total macrocell current varies roughly with the square root of the relative resistivity change ($n \sim -0.5$) and the maximum corrosion current density shows a weaker dependence ($n \sim -1/4$). The total corrosion current is altered the least by changes in resistivity ($n > -1/4$) over the range investigated.

Figure 5 shows a similar treatment to examine the dependence of corrosion severity on the diffusivity of oxygen. The total macrocell current density shows a moderate power dependence ($n \approx 1/2$) with the diffusivity. The total macrocell current density and, importantly, the total

corrosion current show a stronger dependence ($1/2 \approx n \approx 1$) on the diffusivity of oxygen than that shown for the concrete resistivity. The relative importance of concrete resistivity and oxygen diffusivity as corrosion parameters is also shown in Figure 5 by displaying the results of calculations where $\rho_L = 2$ kΩ-cm (solid lines) and $\rho_L = 20$ kΩ-cm (dashed lines). With the exception of the total macrocell current, a relative change in oxygen diffusivity has a greater effect than a similar change in concrete resistivity.

Figure 6 shows the effect of changing the height of the active zone above water on the corrosion severity. The total corrosion current increases with the height of the active zone, as expected since more active material is available for corrosion, in a region where oxygen supply is less restricted than below water. The same happens for the maximum corrosion current density. Interestingly, the total macrocell current changes little with the height of the active zone above water. The corrosion current density distribution associated with this behavior is seen in Figure 7. As the active zone above water becomes shorter, the corrosion current density in the submerged zone becomes greater. In the presence of a sizable active steel zone above water, the oxygen consumed there served to increase the local iron dissolution rate. Without a large active zone above water, the effect of oxygen consumption there is to increase the corrosion rate below water (which was otherwise restricted by the slow local delivery of oxygen through water-saturated concrete). The combination of the system dimensions and the diffusivity and resistivity distributions used here creates an effective limiting current phenomenon, with the resulting observed stability of the total macrocell current. It should be noticed also that the calculated increase in corrosion rate below water is uniform. This results form the assumption of an equipotential concrete surface in the submerged area. Some deviation from this behavior would result if a finite resistivity for seawater were assumed.

Polarization of the Oxygen Reduction Reaction

Further insight on the corrosion process in these systems can be gained by examination of the potential-current relationship of the oxygen reduction reaction. Figure 8 shows a composite E-log i (sum of both sides) curve for the entire column, for the baseline case (A). The more noble potentials correspond to the passive region above water, where diffusional transport is not limiting. As a result, the curve approaches ideal Tafel behavior, with a slope close to the assumed value of 0.16 V per decade. As more active potentials are reached, a diffusional limitation is encountered. However, because the system is three-dimensional and the diffusion coefficient is variable, the curve does not approach a simple limiting current density. The kink in the curve corresponds to the transition into the active portion of the rebar cage. The current density actually decreases dramatically as the potential becomes less noble. Finally, the curve portion representing most of the submerged portion of the column is compressed near the end point (which corresponds to the flat portion of the plots in Figure 3, bottom.) The composite polarization curve illustrates the complexity of the phenomena encountered in large, heterogeneous systems. It should be noted that this curve does not represent the polarization behavior of an individual surface element on the rebar cage; behavior which varies with position along the column length. Rather, the complex nature of the system examined here prevents the use of a master cathodic polarization curve, as is sometimes assumed in the computer modeling of extended structures [12,16].

It should also be noted that the steel in the portion of the column below water, which has the less noble potentials, does not have the highest corrosion rate. This observation is in line with the behavior observed in similar systems [17], and emphasizes the importance of not equating high

corrosion rates with extreme potential readings, as it would result from an uncritical application of specialized corrosion criteria (such as ASTM C-876).

Modeling Considerations

The interpretation of the peak current density magnitudes reported (Figures 3-7) must be qualified by keeping in mind that discretization errors are unavoidable. The peak current densities present at the active-passive transition line would be finite even if a continuous model were used (as required by Eqs. (1) and (2)). However, the computational grid used here prevents obtaining the actual values of the peak current densities at the transition itself, and only values at points half a grid space away can be estimated. The actual value at the transition will differ from the reported value by an amount depending on the effective polarization slope acting at that point, and on the rate of potential variation across the transition. Since the potential tends to vary rapidly across the region of interest, the peak current density results reported here are to be considered as an approximation, useful to evaluate the relative effects of the corrosion parameters of the system. It should also be understood that in a real system a sharply defined spacial active-passive transition is not likely to be present, and that the simulation of a rebar cage by means of a fine mesh has already involved numerous simplifications.

Implications on Marine Substructure Conditions

The calculations provide quantitative support to the long-held view that the corrosion rate in the underwater portion of the structure is small as a result of limited oxygen access. The calculations indicate however that corrosion underwater could be enhanced as a result of corrosion macrocell coupling with the portion above water, if the anodic activity there is lessened. This finding merits consideration if corrosion abatement methods for the splash zone (such as the use of silane or siloxane surface treatments) become successful. The possibility of enhanced corrosion underwater in those cases should be examined in more detail.

The calculations showed that limitation of the oxygen reduction reaction below water need not be due, as sometimes thought, to low availability of oxygen in the seawater itself; oxygen concentrations comparable to those present near the surface are encountered even at great depths [13]. In the computed cases the limitation results from the oxygen diffusion process through the concrete cover. The calculations suggest moreover that oxygen supply from above through the core of the column is not likely to be important to the corrosion behavior underwater.

The quantitative results agreed also with the common observation of severe corrosion in the splash-evaporation zone of marine substructures. Depending on the choice of parameters assumed, macrocell currents ranged from about 10% to 90% of the total corrosion current of the system. In general, total macrocell currents were a larger fraction of the total corrosion current when range of values of the concrete resistivity or the oxygen diffusivity was low. The high calculated corrosion current densities near the top of the active zone resulted from a combination of increasing oxygen diffusivity with height (which allowed for greater local cell action), and coupling with the oxygen reduction at the nearby portion of the passive zone. The "throwing power" of the macrocell effect into the passive zone can be estimated from Figure 3 (bottom) to be on the order of 0.1m to 1m for the conditions investigated. As indicated earlier, the macrocell effect distances could be much larger into the less resistive submerged zone. Other characteristics of the system (such as steel placement density and effective exchange current densities) will be expected to play a role in

determining the extent to which the macrocell action contributes to the overall development of corrosion in the column.

Regardless of the relative importance of local versus extended cell action, the results underscored the importance of increasing concrete resistivity and reducing the effective oxygen diffusivity to lower the overall corrosion rate. The present trend toward using denser concretes in marine construction is therefore expected to be beneficial not only in delaying the onset of active corrosion (by retarding chloride ion ingress), but also because of the reduced gas transport and higher resistivities of those materials [17].

Model Extension and Enhancement

The results presented here covered only some of the most important variables in the problem. The present model is suitable also to evaluate the effect of concrete cover thickness, alternative oxygen diffusivity and concrete resistivity profiles, alternative steel placement density and polarization variables, truncated column geometries and a number of service-related situations. Those conditions should be examined in detail for possible implications on structural design for improved corrosion resistance. The model could also be modified to evaluate the performance of various cathodic protection options; work along those lines is in progress and will be presented elsewhere.

Numerous factors of importance remain unaddressed because of the assumptions of the present model; the following is only a partial account of possible improvements leading to a more realistic simulation. A desirable enhancement would be the implementation of a more realistic rebar geometry simulation. It is expected that the typical three-dimensional cage assembly will give rise to current and oxygen flow concentration effects that may significantly alter the local corrosion distribution from the more uniform conditions examined here. The polarization characteristics assumed here make no allowance for back reactions, which might be important in the submerged zone. The anodic reaction can be very complex and involve several intermediate states not considered here. In addition, the simple active-passive behavior assumed here is a strong simplification of the actual material behavior. The cathodic reaction rate may be strongly sensitive on the surface condition of the steel. and it may also involve other reactions (such as ferric to ferrous ion conversions) not considered here. Reliable data on oxygen diffusivity in concrete are scarce, and in view of the importance of that parameter suggested by the results, more documented information may be highly beneficial in that area.

CONCLUSIONS

1. In a simulated reinforced concrete marine substructure column, the potential of the reinforcing steel varied continuously from the noble values in the zone above water to very active values in the submerged zone.

2. The concentration of oxygen inside the column varied from a value near equilibrium with the exterior at the top, to almost zero below water. Oxygen transport to the steel below water was almost exclusively through the concrete cover and not downward through the center of the column.

3. The corrosion current density was greatest at the top of the active zone of the column. Corrosion below water proceeded at a smaller rate even though the steel potential was significantly

less noble than in the region of highest corrosion.

4. The local oxygen consumption rate was greatest near the top of the active steel zone. This resulted from a combination of the oxygen diffusivity pattern assumed in the calculations, and of the proximity of the active steel zone.

5. The total corrosion current varied from being almost equal to the total macrocell current, to being several times greater, depending on the values of concrete resistivity and oxygen diffusivity ranges assumed. Low concrete resistivities, or low oxygen diffusivities, tended to reduce the relative difference between total corrosion current and macrocell current.

6. Corrosion below water was not enhanced by oxygen consumption in the air zone unless corrosion activity in the latter was greatly reduced. This suggests that undesirable side-effects of reducing corrosion in the air zone might occur and should be investigated.

7. The overall level of corrosion increased with increasing oxygen diffusivity and reduced concrete resistivity.

8. Relative changes in oxygen diffusivity had a greater impact on corrosion activity than comparable relative changes in concrete resistivity.

9. The three dimensional, heterogenous nature of the system leads to polarization behaviors that cannot be described by a simple monotonic polarization curve.

ACKNOWLEDGMENTS

This investigation was supported by the Florida Department of Transportation (FDOT) in cooperation with the U.S. Department of Transportation (USDOT). The opinions, findings and conclusions expressed in this document are those of the authors and not necessarily those of the FDOT or USDOT. The authors are also indebted to the University of South Florida Engineering Computing Services for access to their facilities and support.

NOMENCLATURE

b_a Activation Tafel slope for the anodic reaction.

b_c Activation Tafel slope for the cathodic reaction.

c Concrete cover.

C Oxygen concentration.

C_s Oxygen concentration at the steel surface.

C_O Oxygen concentration at the external concrete surface.

D Oxygen diffusion coefficient.

D_H. D_L	Highest and lowest values of D.
E	Potential at a point of the electrolyte (through an idealized reference electrode) with respect to the body of the metal. Note that this convention, used throughout this paper, is the opposite of the common usage of referring potentials with respect to a reference electrode placed in the electrolyte.
E_s	Potential at the electrolyte immediately next to the metal surface.
$E_{o\ Fe}$	Redox potential for the $Fe/Fe^{++}+2e$ system.
$E_{o\ OR}$	Redox potential for the OH^-/O_2+2H_2O+4e system.
h_A	Height of active zone above water.
i_{Fe}	Current density of the iron oxidation reaction.
i_{OR}	Current density of the oxygen reduction reaction.
$i_{o\ Fe}$	Exchange current density for the $Fe/Fe^{++}+2e$ system.
$i_{o\ OR}$	Exchange current density for the OH^-/O_2+2H_2O+4e system.
i_{CORR}	Corrosion current density.
I_{CORR}	Corrosion current.
I_{MACRO}	Macrocell current.
i	Current density vector.
L	Column length.
n	Direction normal to a surface, pointing away from the surface.
r	Radial column direction.
w	Column diameter.
z	Axial column direction.
$\nabla\|_p A$	Component along the direction p of the gradient of scalar magnitude A.
ρ	Concrete resistivity.
ρ_H, ρ_L	Highest and lowest values of ρ.
σ	Concrete conductivity ($\sigma = 1/\rho$)

BIBLIOGRAPHY

1. Macias, A., and Andrade, C. , Corrosion Sci., Vol 30, p.393, 1990.

2. "Corrosion of Metals in Concrete", ACI Journal Committee Report by ACI Comm. 222, Journal of the American Concrete Institute, p.3, Proceedings Vol.82, 1985.

3. Slater, J., "Corrosion of Metals in Association with Concrete", ASTM STP 818, ASTM, Philadelphia, 1983.

4. Sagüés, A. , Perez-Duran. H. and Powers, R., Corrosion, Vol 47, p.884, 1991.

5. Gjorv, O., Vennesland, O. and El-Busaidy, A., Materials Performance, Vol.25, No.12, p.39 (1986).

6. Tuutti, K., Corrosion of Steel in Concrete, Swedish Cement and Concrete Research Institute, 1982.

7. Strattful, R., Materials Protection, p. 29, March 1968.

8. Millard, S. G., Ghassemi, M., Bungey, J. and Jafar, M., "Assessing the Electrical Resistivity of Concrete Structures for Corrosion Durability Studies", in Corrosion of Reinforcement in Concrete, C. Page, K. Treadway and P. Bamforth, Eds., p.303, Elsevier Appl. Sci., London-New York, 1990.

9. Kranc, S.C. and Sagüés, A.A., "Computation of Corrosion Macrocell Current Distribution and Electrochemical Impedance of Reinforcing Steel in Concrete", in Computer Modeling in Corrosion, ASTM STP 1154, R.S. Munn, Ed., American Society for Testing and Materials, Philadelphia, p.95, 1992.

10. Kranc, S.C. and Sagüés, A.A., "Calculation of Extended Counter Electrode Polarization Effects on the Electrochemical Impedance Response of Steel in Concrete", in Electrochemical Impedance: Interpretation and Analysis, ASTM STP 1188, D.C. Silverman, J.R. Scully and M.W. Kendig, Eds., American Society for Testing and Materials, Philadelphia, 1993.

11. Sagüés, A. and Kranc, S.C., Corrosion, Vol. 48, p.624, 1992.

12. Naish, C., Harker, A. and Carney, R., "Concrete Inspection: Interpretation of Potential and Resistivity Measurements", in Corrosion of Reinforcement in Concrete, C. Page, K. Treadway and P. Bamforth, Eds., p.314, Elsevier Appl. Sci., London-New York, 1990.

13. Shreir, L., Editor, Corrosion, Volume 2, Corrosion Control, p.21:56, Newnes-Butterworths, London, 1976.

14. Sagüés, A., "Mechanism of Corrosion of Epoxy-Coated Reinforcing Steel in Concrete", Final Report No. FL/DOT/RMC/0543-3296, National Technical Information Service, Springfield, VA 22161, April 1991.

15. Clear, K. Measuring Rate of Corrosion of Steel in Field Concrete Structures, TRB 68th Annual Meeting, January 22-26, 1989, Paper Preprint No. 88-0324.

16. Munn, R.S., Editor, "Computer Modeling in Corrosion", ASTM STP 1154, American Society for Testing and Materials, Philadelphia, 1992.

17. Browne, R., "Mechanisms of Corrosion of Steel in Concrete in Relation to Design, Inspection and Repair of Offshore and Coastal structures", in Performance of Concrete in Marine Environment, Publication SP-65, American Concrete Institute, Detroit, 1980.

18. Millard, S.G., Durability Performance of Slender Reinforced Coastal Defense Units, in Concrete in Marine Environment, p.339, V. Malhotra, Ed., ACI SP-109, American Concrete Institute, Detroit, 1988.

TABLE I
CASES INVESTIGATED

CASES	h_A (cm)	D_L (cm^2/s)	D_H (cm^2/s)	ρ_L (kΩ-cm)	ρ_H (kΩ-cm)
A BASELINE	202.5	10^{-5}	10^{-3}	2	10
B	202.5	10^{-5}	10^{-3}	20	100
C	102.5	10^{-5}	10^{-3}	2	10
D	2.5	10^{-5}	10^{-3}	2	10
E	302.5	10^{-5}	10^{-3}	2	10
F	202.5	10^{-6}	10^{-4}	2	10
G	202.5	10^{-7}	10-5	2	10
J	202.5	10^{-6}	10^{-4}	20	100
K	202.5	10^{-7}	10^{-5}	20	100
L	202.5	10^{-5}	10^{-3}	6	30
M	202.5	10^{-5}	10^{-3}	1	5

For all cases:

L = 1200 cm
w = 105 cm
c = 10.5 cm
$i_{o\,Fe}$ = $1.875\ 10^{-8}$ A/cm^2
$i_{o\,OR}$ = $6.25\ 10^{-10}$ A/cm^2
$E_{o\,Fe}$ = 780 mV*
$E_{o\,OR}$ = -160 mV*
b_a = 60 mV
b_c = 100 mV
C_O = $3\ 10^{-7}$ Mol/cm^3

* SCE scale, signs per convention in Nomenclature section.

TABLE II
SELECTED CALCULATED MAGNITUDES

CASE	TOTAL MACROCELL CURRENT (mA)	TOTAL I_{CORR} (mA)	MAXIMUM i_{CORR} ($\mu A/CM^2$)	OXYGEN CONSUMED BELOW WATER (mA)	IRON DISSOLVED BELOW WATER (mA)
A BASELINE	14.2	49.7	4.5	19.6	20.2
B	3.89	39.8	2.2	19.6	20.0
C	13.7	38.4	3.3	19.6	21.8
D	14.2	34.1	0.57	19.6	34.1
E	14.3	73.5	6.5	19.6	18.9
F	5.8	9.3	1.4	0.91	1.51
G	2.48	2.7	0.35	0.196	0.44
J	2.05	5.64	0.6	1.96	2.25
K	0.76	1.11	0.17	0.196	0.236
L	8.05	43.5	3.2	19.6	20.1
M	20.5	57	5.52	19.6	20.7

(rates correspond to the sum of both sides)

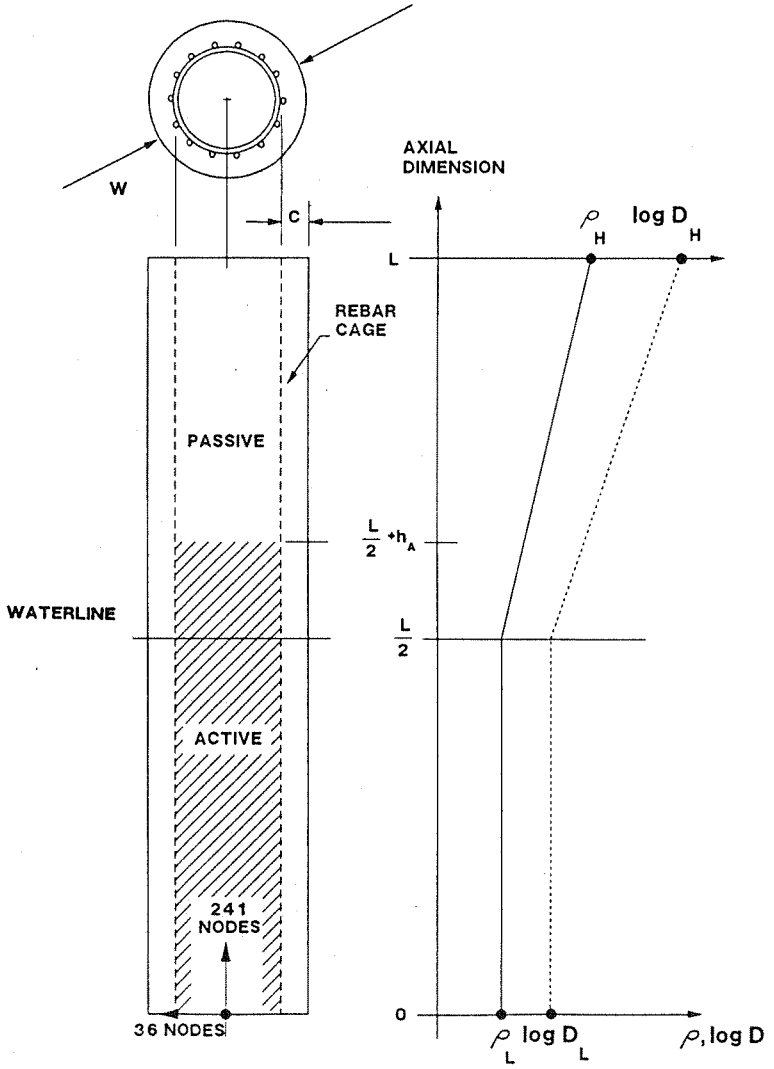

Figure 1. Idealized, half submerged reinforced concrete column model.

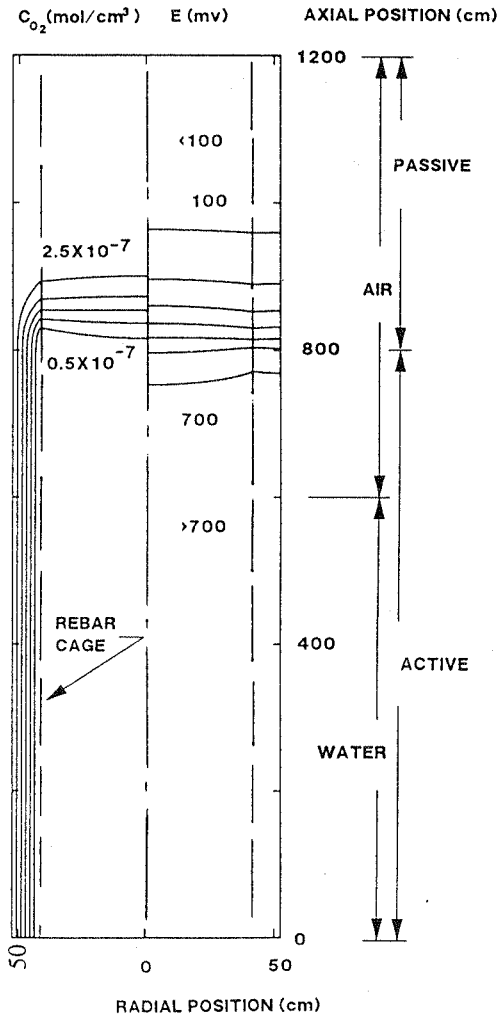

Figure 2. Isopotential and isoconcentration lines showing the results of the model calculations for the baseline case A. The equipotential lines are separated at equal intervals of 100 mV each. The isoconcentration lines are 0.5 10^{-7} Mol/cm^3 apart.

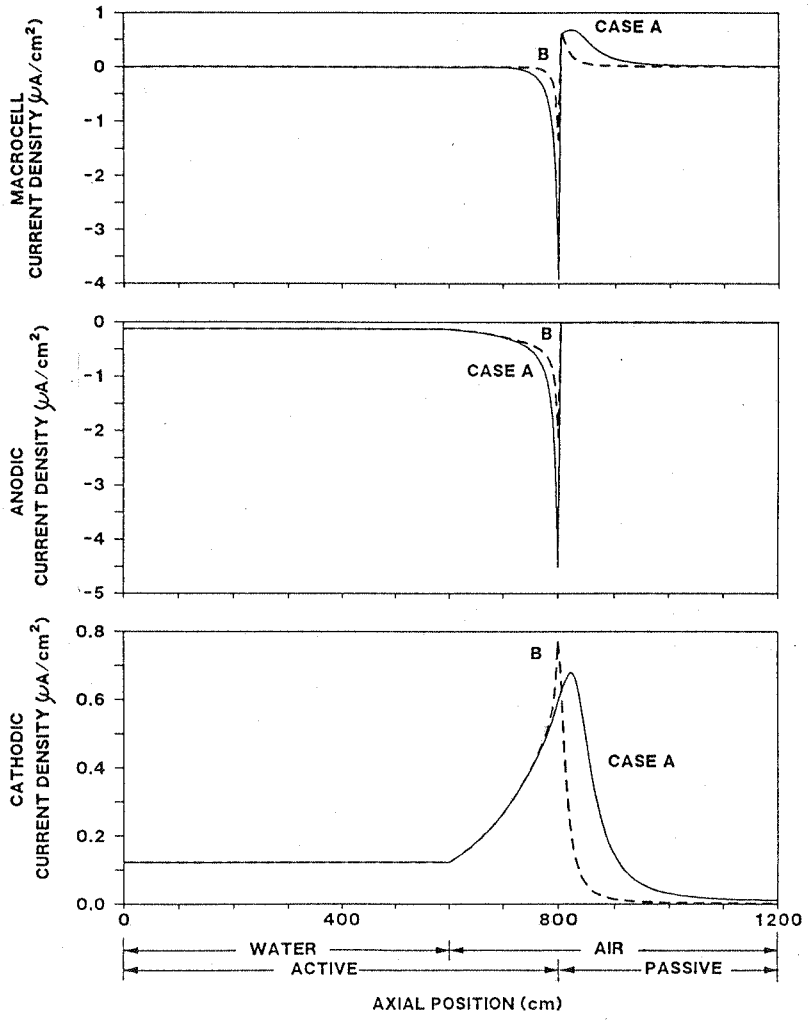

Figure 3. Current density (sum of both sides) distributions along the rebar cage for the baseline case A and for case B (higher concrete resistivity). The macrocell current density (top) is equal to the algebraic sum of the anodic (center) and cathodic (bottom) current densities. The absolute values of the corrosion current density and the oxygen consumption current densities are equal to those of the anodic and cathodic current densities respectively.

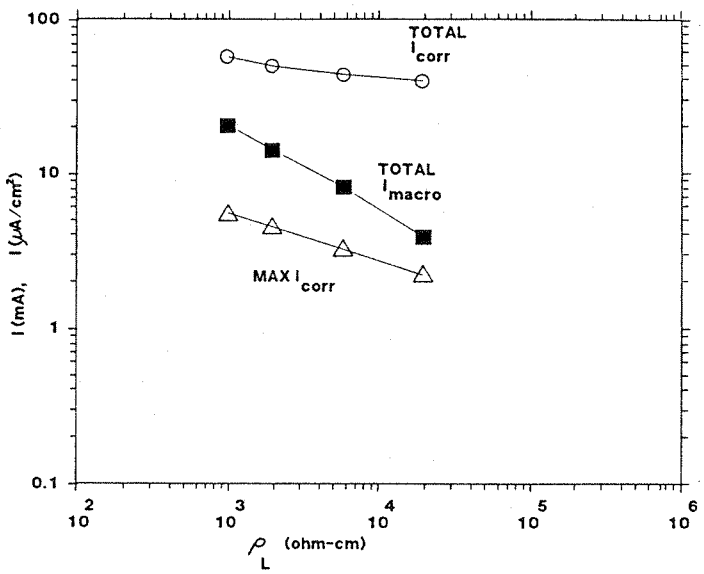

Figure 4. Total corrosion and macrocell currents, and maximum corrosion current density (sums of both sides), as a function of lowest concrete resistivity while keeping the other parameters constant (results from cases A,B,L and M).

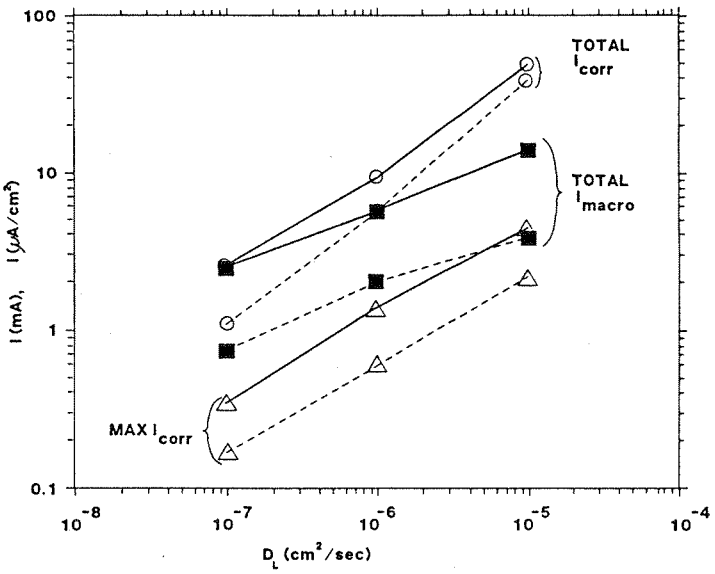

Figure 5. Total corrosion and macrocell currents, and maximum corrosion current density (sums of both sides) as a function of lowest concrete diffusivity while keeping the size of the active and passive regions constant. The solid lines, filled symbols, correspond to the cases with the resistivity range 2-10 KΩ-cm (A,F,G). The dashed lines, open symbols correspond to the cases with the resistivity range 20-100 KΩ-cm (B,J and K).

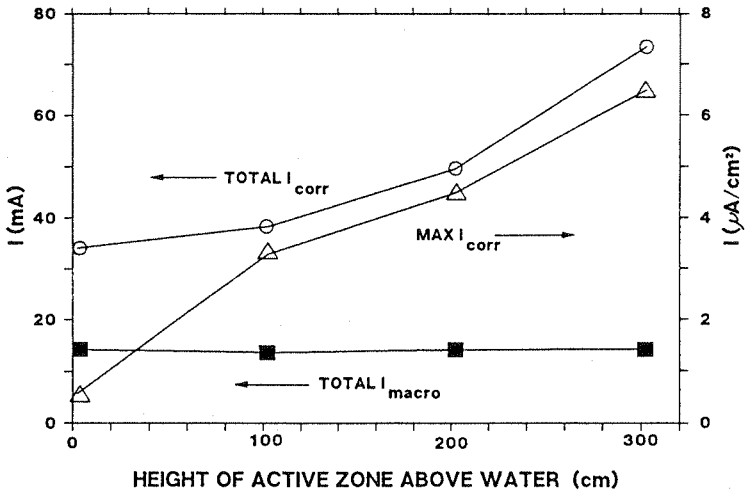

Figure 6. Total corrosion and macrocell currents, and maximum corrosion current density (sums of both sides), as a function of height of the active zone above water while keeping the other magnitudes constant (cases A,C,D and E).

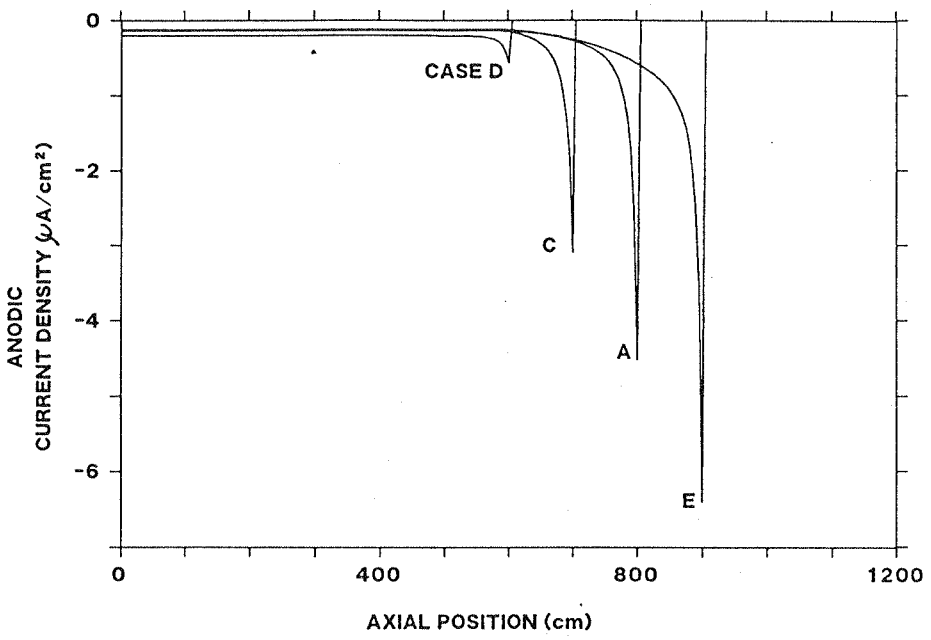

Figure 7 Distribution of the corrosion current density (sums of both sides) for the cases indicated in Figure 6.

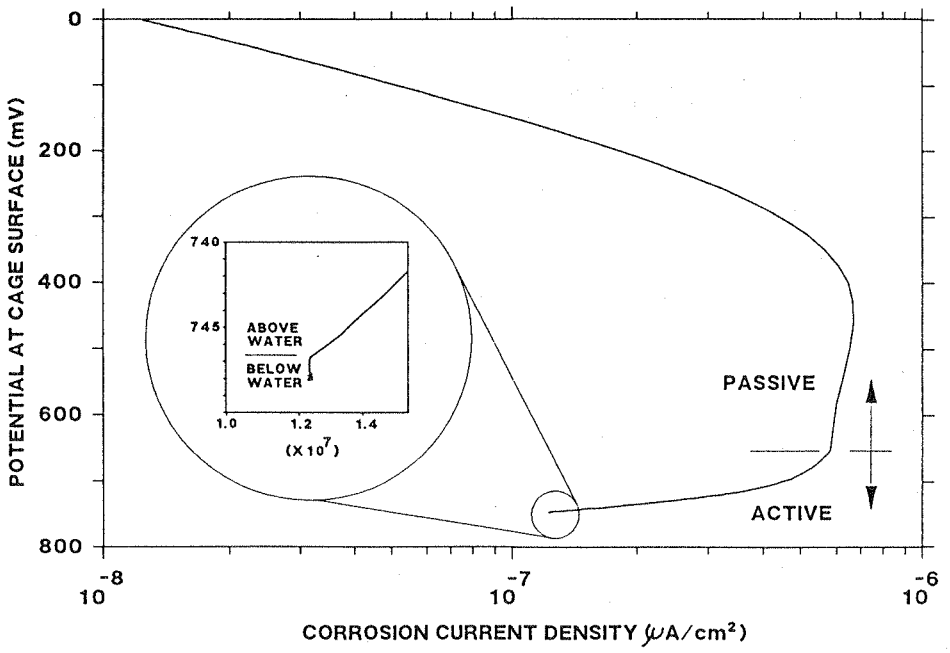

Figure 8. Composite polarization diagram showing the locus of potential at the cage surface and oxygen consumption current density (sum of both sides) as it varies along the rebar cage (baseline case A). The portions of the diagram corresponding to different column regions are indicated in the main plot and in the detailed inset.